ACCSCIENCE PUBLISHING

International Journal of Bioprinting

RESEARCH ARTICLE

High-resolution 3D printing of collagen I-based scaffolds via Schiff-base interaction for enhanced osteogenic differentiation

Kaixuan Li[1,2†], Hanxiao Huang[1,2,3†], Peng Ge[1,2], and Cailiang Shen[1,2*]

[1]Department of Orthopedics, The First Affiliated Hospital of Anhui Medical University, Hefei, Anhui, China

[2]Laboratory of Spinal and Spinal Cord Injury Regeneration and Repair, Department of Spine Surgery, The First Affiliated Hospital of Anhui Medical University, Hefei, Anhui, China

[3]Department of Stomatology, The First Affiliated Hospital of Anhui Medical University, Hefei, Anhui, China

Abstract

Collagen I is a key extracellular matrix (ECM) component in bone tissue and one of the most important biomaterials for bone tissue engineering applications. However, printing high-resolution mesh scaffold from collagen I remains challenging due to its relatively weak ink shape fidelity. While previous efforts have attempted to improve printability by increasing ink viscosity, such approaches often compromise ink flowability and yield only modest improvements in printing resolution. To solve this issue, we blended oxidized cellulose with collagen I to form a Schiff-base interaction. The resulting hydrogel exhibited lower viscosity but a more apparent linear rheological characteristic, as demonstrated by our large amplitude oscillation sweep results. This enhanced rheological profile enabled the fabrication of scaffolds with a printing resolution approaching 150 μm—one of the highest reported for collagen I-based scaffolds. Scaffolds with this scale of rod diameter and pore size greatly enhanced the proliferation and osteogenic differentiation of mesenchymal stem cells. Correspondingly, the expression of key osteogenic markers, including N-cadherin, HIF-1α, and β-catenin, was upregulated. These findings broaden our understanding of scaffold design and processing optimization of collagen I-based scaffolds and may advance their application in bone tissue engineering.

Keywords: 3D printing; Collagen I; Osteogenic differentiation; Printing resolution

†These authors contributed equally to this work.

***Corresponding author:**
Cailiang Shen
(shencailiang@ahmu.edu.cn)

Citation: Li K, Huang H, Ge P, Shen C. High-resolution 3D printing of collagen I-based scaffolds via Schiff-base interaction for enhanced osteogenic differentiation. *Int J Bioprint*. 2025;11(4):225-241. doi: 10.36922/IJB025140116

Received: April 1, 2025
1st revised: May 23, 2025
2nd revised: May 28, 2025
Accepted: May 29, 2025
Published online: June 3, 2025

1. Introduction

Collagen I is a key extracellular matrix (ECM) compound in bone tissue and has been considered one of the most ideal biomaterials for bone tissue engineering.[1,2] It is highly biocompatible and contains surface Arg-Gly-Asp (RGD) groups that bind to specific cell receptors, promoting cell adhesion.[3,4] Therefore, it is superior to general thermoplastic biopolymers and ceramics for a broad field of tissue engineering applications. Also, collagen I has been shown to promote osteogenic differentiation of stem cells more effectively than many other natural biopolymers like gelatin.[5] For these reasons,

some studies have blended it with other biopolymers or ceramics to produce bone tissue scaffolds.[6–9] However, printing a high-resolution scaffold composed of collagen I is challenging, presumably due to its weak gelation strength, especially in comparison to gelatin.[10,11] While gelatin macromolecules undergo a unique transition from random flexible coils to rigid triple helix structures under cooling, this process does not occur in collagen I.[12] Instead, its viscosity increases only through greater chain entanglement at lower temperatures.[13] As a result, the shape fidelity of collagen I-based hydrogels is relatively weak, yielding generally poor printing resolution. High scaffold resolution is crucial to provide a large surface area for cell adhesion, absorption of nutrition and growth factors, and biochemical reactions necessary for ECM synthesis,[14,15] as well as to generate a high number of rod junctions to facilitate cell migration according to the Random Walk Model.[16] Therefore, it is important to achieve high resolution with collagen I-based scaffolds so that both structural and compositional characteristics can be optimized simultaneously.

To achieve this goal, recent studies have utilized cryogenic printing to facilitate ink solidification. In this process, the hydrogel ink is printed onto a readily-cooled 2D plate or into a 3D well.[6,17–20] To further improve the printing performance, some studies attempted to use lower temperatures or added rigid nanoscale fillers to maximize viscosity.[21–23] Although these approaches improve the shape fidelity and printing resolution to some extent, achieving a resolution finer than 200 μm remains difficult.[6,17–20] Also, increasing ink viscosity inevitably reduces flowability, complicating extrusion and reducing the continuity and uniformity of the printed structures.[24,25]

Given the low strength of the hydrogel formed by collagen I macromolecular entanglement, a promising solution is to introduce external bonding for stabilization. Among the commonly applied chemical modifications for hydrogel rheology, Schiff-base interactions are frequently used. This reversible bonding can be weakened by shear stress during extrusion and reformed afterward. So, Shiff-base hydrogels exhibit shear-thinning behavior, maintaining both flowability and shape fidelity.[26] Some recent studies have applied Shiff-base interactions to gelatin-based hydrogels, resulting in increased ink rigidity and mechanical properties.[27–30] Following this principle, we introduced Schiff-base interactions into a collagen I-based hydrogel to study its effects on rheological properties, printing performances, and its ability to promote mesenchymal stem cell (MSC) proliferation and osteogenic differentiation—assessing its potential prospects in bone tissue engineering.

In this study, we overcame the hurdle of printing high-resolution natural hydrogel-based mesh scaffolds by blending oxidized cellulose and collagen I to form a hydrogel ink with Schiff-base interactions and printing it under cryogenic conditions. The resulting scaffolds featured pore and rod sizes as small as 150 μm. We investigated how these dimensions influenced MSC proliferation and osteogenic differentiation, and discussed the possible underlying mechanisms. This study not only advances the understanding of optimal scaffold dimensions for osteogenic differentiation but also achieves simultaneous optimization of scaffold composition and structure. We believe this work contributes significantly to scaffold design and optimization for bone tissue engineering applications.

2. Materials and methods

2.1. Materials

Collagen I, alginate (β-D-mannuronicacid/-L-guluronicacid ratio (M/G) = 1:1), gelatin (gel strength ~200 Bloom, biotech grade), sodium peroxide, genipin, and anhydrous calcium chloride ($CaCl_2$) were all supplied by Macklin (China). Hydroxymethyl cellulose was provided by Sigma Aldrich (USA).

2.2. Oxidation of cellulose and preparation of hydrogel inks

Hydroxymethyl cellulose was dissolved in deionized water in a 4% w/v concentration (4 g in every 100 mL of water) in a 100 mL flask. The solution was heated at 37°C for 1 h and stirred constantly with a magnetic bar. Then, 0.2 w/v sodium peroxide was added to the solution in a dark environment, and the solution was stirred at 40°C for 1 h. The resulting solution was denoted as "oxidized cellulose solution". A schematic of the reactions is shown in Figures 1 and 2. Then, 8% w/v collagen I and 8% w/v gelatin was added to the oxidized cellulose solution by stirring at 37°C for 1 h. Lastly, 25% w/v alginate was added to each solution and stirred at 37°C for 1 h. For the collagen I-based hydrogel inks, the ink containing non-oxidized cellulose was denoted as "ink A," while the ink containing cellulose oxidized by sodium peroxide was denoted as "ink B". In the meantime, a crosslinking solution was prepared by dissolving 2% w/v genipin and 20% w/v $CaCl_2$ in deionized water. Fourier transform infrared spectroscopy (FTIR) characterization was performed on hydrogels containing ink A or B using a Bruker FTIR instrument (Germany).

2.3. 3D printing and post-treatment handling

3D printing was conducted with an extrusion-based 3D printer (Regenovo, China). The printer was equipped with a 3D cryogenic well, and the extrusion force was driven by compressed air. Tapered plastic needles were used for

printing (inner diameter: 200 μm; outer diameter: 220 μm). The temperature of the 3D cryogenic well was set to −1°C for printing both collagen I and gelatin-based inks, and a total of seven layers were printed with each ink. Three samples were printed using ink B and with rod distances (distance between the centerline of adjacent rods) of 300, 450, and 600 μm, and were denoted as "sample 1," "sample 2," and "sample 3", respectively. Another scaffold was printed with gelatin-based ink and a rod distance of 600 μm, denoted as "sample 4". The layer height and extrusion pressure were both set to 0.14 mm. The printing pressure was set to 0.18 MPa for printing collagen I-based ink and 0.25 MPa for printing gelatin-based ink. Upon the completion of printing, the crosslinking solution was added dropwise to the scaffolds until fully immersed. The scaffolds were then removed and stored in a refrigerator at −20°C.

2.4. Morphological study

All printed scaffolds were freeze-dried and loaded into the chamber of a scanning electron microscope (SEM; Zeiss, Germany) and vacuumed again. SEM observation was conducted under a secondary electron (SE) mode with an accelerating voltage of 3kV. ImageJ software (1.8.0, National Institute of Health, USA) was used to analyze the average rod diameter and pore size of all scaffolds.

2.5. Rheology

Rheological studies were conducted with an Anton Paar MCR 302e rheometer (Anton Paar, Austria), equipped with a 25 mm parallel plate and an isothermal chamber. Inks A and B were tested to evaluate the effect of Schiff-base formation on improving ink shape fidelity. Steady-shear flow test was performed from 0.1 to 100 s^{-1} at −1°C for each ink. An oscillation temperature sweep test was conducted from 37 to −5°C at a constant frequency of 1 rad/s and a strain of 0.5%. Lastly, a large amplitude oscillation sweep (LAOS) test was conducted at a constant frequency of 1 rad/s across a strain range of 0.1–1000%.

2.6. Thermal study

Differential scanning calorimetry (DSC) test was conducted on hydrogel ink A and B using a HITACHI DSC 200 instrument (HITACHI, Japan) under a nitrogen environment. A cooling process from 30 to −10°C was applied at a rate of 1°C/min.

2.7. Mechanical study

Tensile tests were conducted on scaffold samples 1–4 using a universal test machine (UTM 4103, Shenzhen SUNS Technology Stock Co., Ltd., China). A loading rate of 1 mm/min was applied, and each group of scaffolds was tested in triplicate.

2.8. Cell culture and characterizations

2.8.1. Cell seeding

MSCs were extracted from 2-week-old Sprague Dawley mice. Before seeding cells, all scaffolds (samples 1–4) were immersed in 75% ethanol for 10 min, washed once with phosphate-buffered saline solution (Beyotime, China), exposed to UV radiation for 30 min, and immersed in an (α-MEM) Minimum Essential Medium (Vivacell, China) containing 10% fetal bovine serum (Gibco, Australia), penicillin (10 kU/mL) and 10 mg/mL streptomycin solution (10 mg/mL, Beyotime, China) for 24 h. This modified medium was denoted as "complete medium". MSCs (passage 2) were seeded onto the scaffolds at a density of 10^6 cells/mL. Cell culture was conducted in an incubator (Thermo Fisher Scientific, USA) at 37°C with 5% CO_2. After 24 h, once cell adhesion was observed, the complete medium was replaced with an osteogenic induction medium containing an additional 50 μM ascorbic acid, 10 mM β-glycerol phosphate, and 100 nM dexamethasone (all from Sigma Aldrich, USA).

2.8.2. Cell counting kit-8 test

On days 1, 3, and 5 of culture, a cell counting kit (CCK)-8 test was conducted to assess cell proliferation. The α-MEM medium containing 10% CCK-8 cell counting agent (Beyotime, China) was added and incubated for 1 h. A total of 100 μL of cell supernatant was used to measure the Optical Density (OD) value at a wavelength of 450 nm using a spectrophotometer (Multiskan GO, Thermofisher Scientific, USA).

2.8.3. Cell morphology staining

MSCs were seeded onto scaffolds placed in a 24-well plate. Actin-Tracker Red (Beyotime, China) and 4'6-diamidino-2-phenylindole (DAPI; Beyotime, China) were used for immunofluorescence staining to visualize the cytoskeleton and nuclei, respectively. An upright fluorescence microscope (DM6 B, Leica, Germany) was used for observation. The excitation/emission wavelengths were 496/516 nm for Actin-Tracker Red and 480/340 nm for DAPI, respectively.

2.8.4. Western blot

On days 7 and 21 of cell culture, protein was extracted from MSCs. Cells were lysed in Radio Immunoprecipitation Assay (RIPA) buffer (Beyotime, China), and total protein concentration was determined using the Bradford assay (Sangon Biotech, China). Protein of equal amounts was separated on a 12% Sodium Dodecyl Sulfate Polyacrylamide (SDS-PAGE) Gel Electrophoresis gel and transferred onto a 0.22 μm-pore size polyvinylidene difluoride membrane (Sigma-Aldrich, USA) under a constant current of 252 mA. The membranes were then blocked with 5% skim milk

and incubated overnight at 4°C with primary antibodies targeting N-cadherin (NCAD), alkaline phosphatase (ALP), osteocalcin (OCN), hypoxia-inducible factor 1α (HIF-1α), β-catenin, and GADPH. After being washed three times with Tris-buffered saline with Tween-20 (Beyotime, China), the membranes were incubated at room temperature with horseradish peroxidase-conjugated secondary antibodies for 1.5 h. Lastly, an enhanced chemiluminescence detection kit (Beyotime, China) was used to visualize the immunoreactive bands.

2.9. Statistical analyses

Each experiment was performed independently in a minimum of three replicates. Statistical analyses were conducted using either Student's *t*-test or one-way analysis of variance, as appropriate, to evaluate differences between treatment groups. All analyses were performed using GraphPad Prism 7 (GraphPad Software, Inc., USA). The *p*-value less than 0.05 was considered statistically significant.

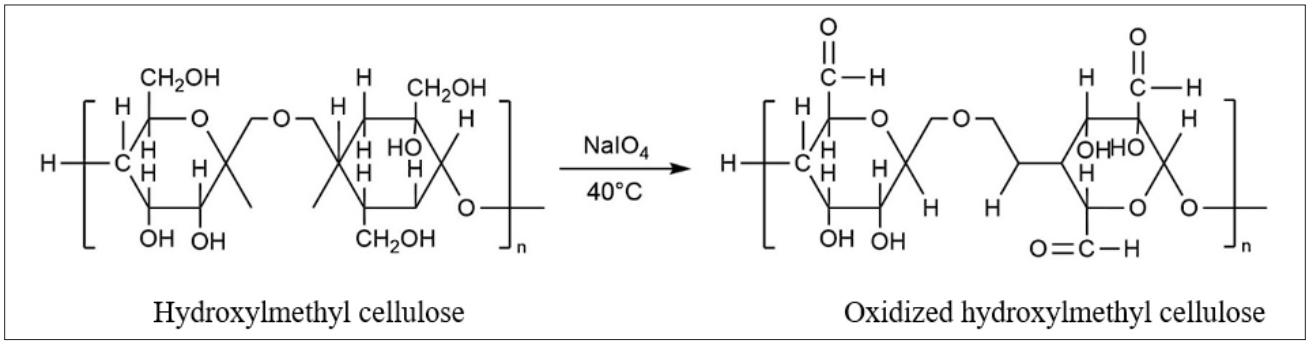

Figure 1. A schematic of cellulose oxidization. Abbreviation: $NaIO_4$, sodium periodate.

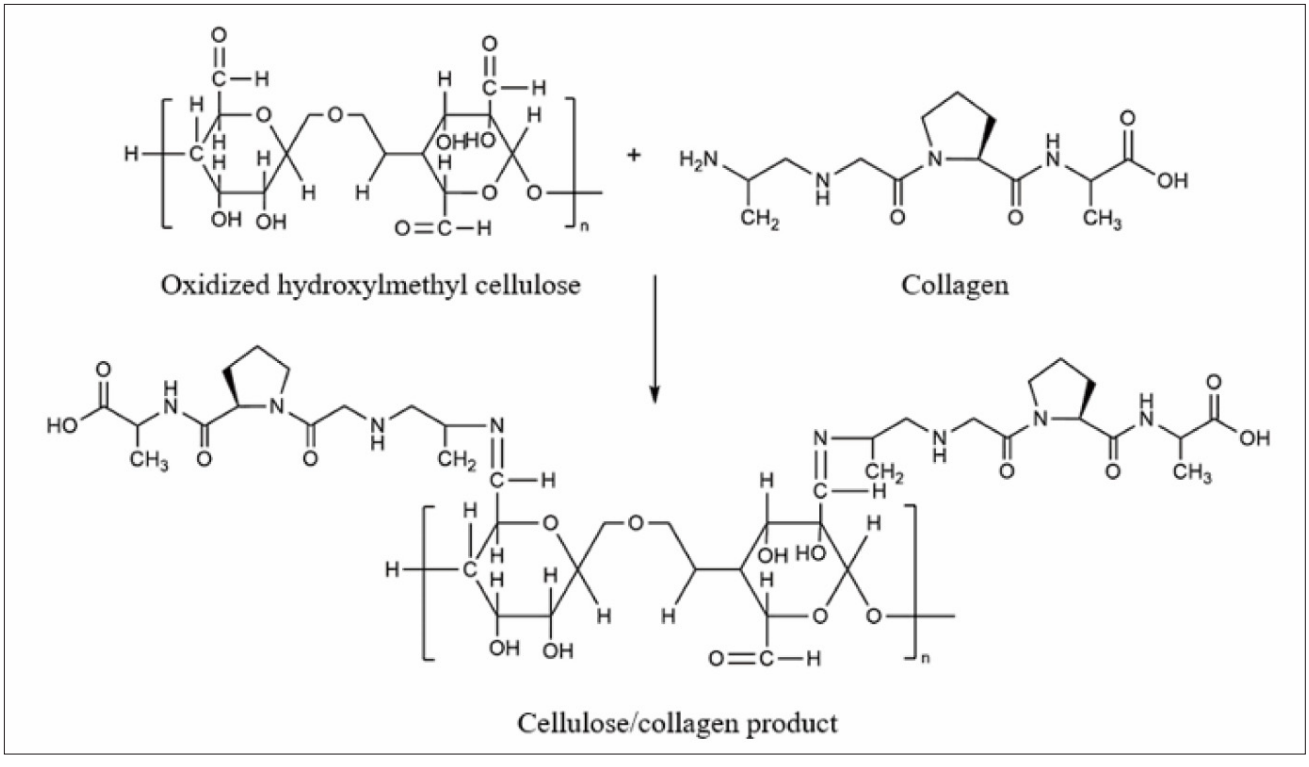

Figure 2. A schematic of Schiff-base interaction formation between collagen and hydroxylmethyl cellulose

3. Results

3.1. FTIR analysis

Following the oxidation of cellulose by sodium peroxide, the hydroxyl groups (–OH) were converted to aldehyde groups. In the FTIR spectra, ink A showed a characteristic –OH peak at 1075 cm^{-1},[31] which was markedly reduced in ink B, indicating successful oxidation. In addition, the characteristic amide peak of collagen I at 1542 cm^{-1} was prominent in ink A but nearly absent in ink B (Figure 3), suggesting its consumption via Schiff-base reactions.[32]

3.2. Rheological study

At the printing temperature of –1 °C, ink A exhibited higher viscosity than ink B. This was consistent with its lower tan δ value and steeper stress–strain curve slope, indicating greater stiffness (Figures 4 and 5). Both inks demonstrated shear-thinning behavior, as viscosity decreased monotonically with increasing shear rate (Figure 4B). LAOS analysis revealed more flattened Lissajous curves for ink B compared to ink A, indicating more linear viscoelastic behavior (Figure 6A). Additionally, ink B showed A higher strain-hardening ratio (Figure 6B), suggesting better structural recovery and printability. The greater linear rheological characteristic of ink B may contribute to its improved shape fidelity during printing.

3.3. Morphological study

Cryogenic 3D printing (Figure 7) was attempted using ink A and B. An optimum combination of pressure and speed parameters was evaluated for each ink until rod breakage occurred. Printing with ink A was more challenging due to its weaker gelation strength, which limited resolution improvements at higher printing speeds and led to frequent rod breakage (Figure 7B). In contrast, ink B enabled smoother printing, likely due to Schiff-base-induced structural reinforcement (Figure 7C). As a result, samples 1–3 scaffolds were printed using ink B, while sample 4 was printed using a gelatin-based hydrogel ink.

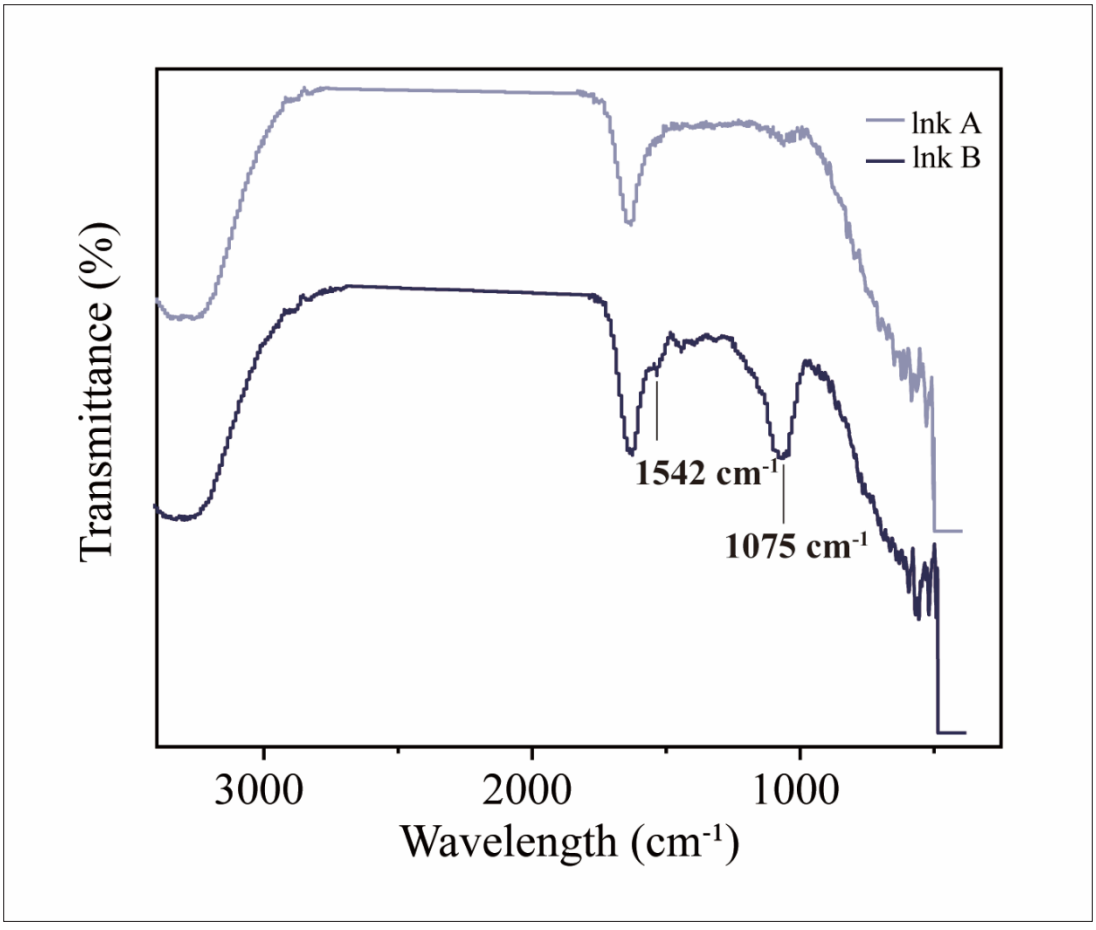

Figure 3. FTIR spectra for ink A (cellulose/collagen I/alginate hydrogel) and B (oxidized cellulose/collagen I/alginate hydrogel). Abbreviation: FTIR: Fourier transform infrared spectroscopy.

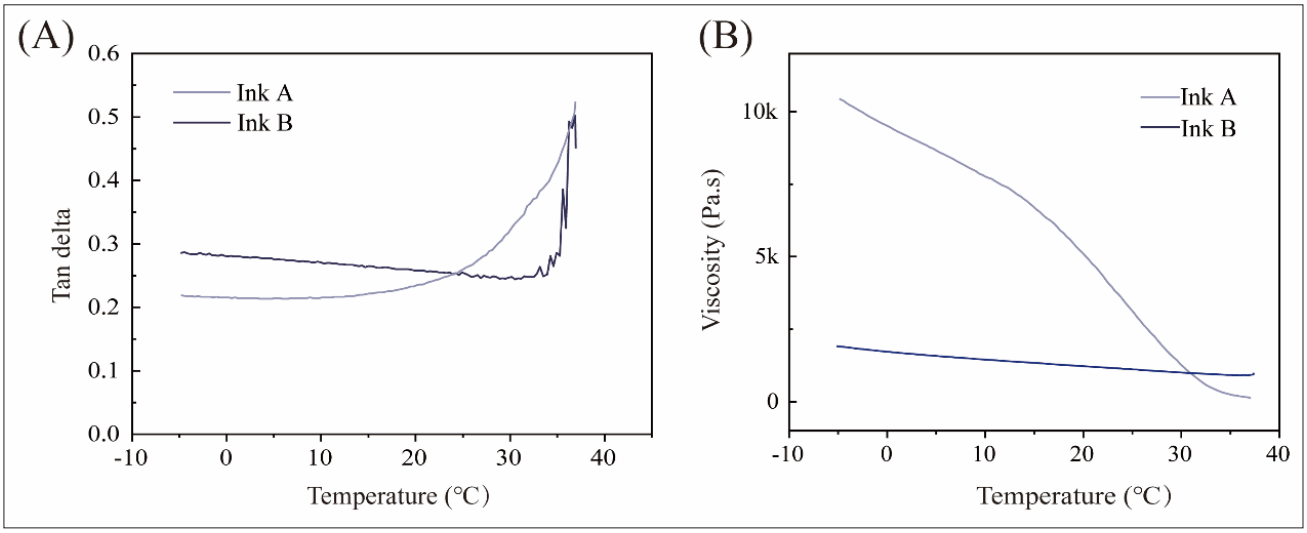

Figure 4. Oscillatory temperature sweep test results for hydrogel inks. Tan δ versus temperature curve (A) and dynamic viscosity versus temperature (B) for ink A (cellulose/collagen I/alginate hydrogel) and B (oxidized cellulose/collagen I/alginate hydrogel).

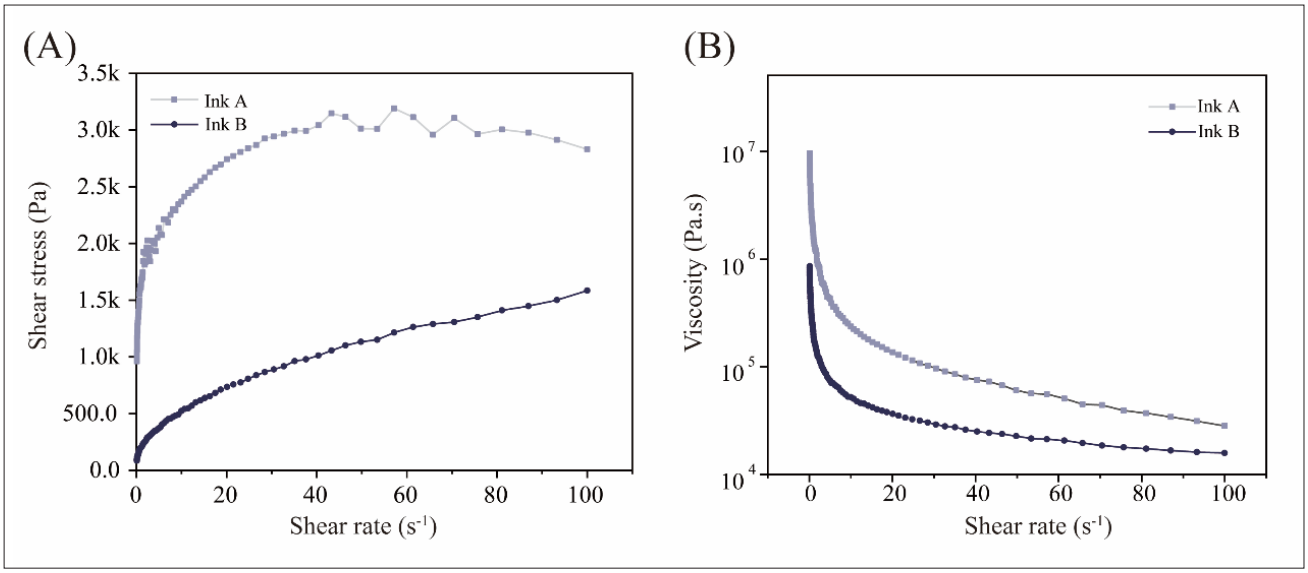

Figure 5. Steady shear flow test results for hydrogel inks. Shear stress versus shear rate curve (A) and viscosity versus shear rate curve (B) for ink A (cellulose/collagen I/alginate hydrogel) and B (oxidized cellulose/collagen I/alginate hydrogel).

The microstructures of samples 1–4 were examined using SEM (Figure 8), and the average rod diameter and pore size were recorded (Table 1). The printing resolution approached 150 μm, representing one of the highest printing resolutions reported for collagen I-based scaffolds to date.[33]

To evaluate the dimensional stability during cell culture, microscale images of the scaffolds were also captured post-swelling (Figure 9). As shown in Table 1, only minor increases in rod diameter were observed, whereas the pore size exhibited slightly greater expansion. Overall, the swelling extent across samples 1–4 was significantly lower than typically reported values, which often exceed 100–200% dimensional increase.[34,35] This stability is likely attributable to the Schiff-base interactions between oxidized cellulose and collagen I.

3.4. Thermal study

The DSC curves for ink A and B are shown in Figure 10. Neither formulation exhibited an apparent phase transition process in the cooling process. Therefore, the printability

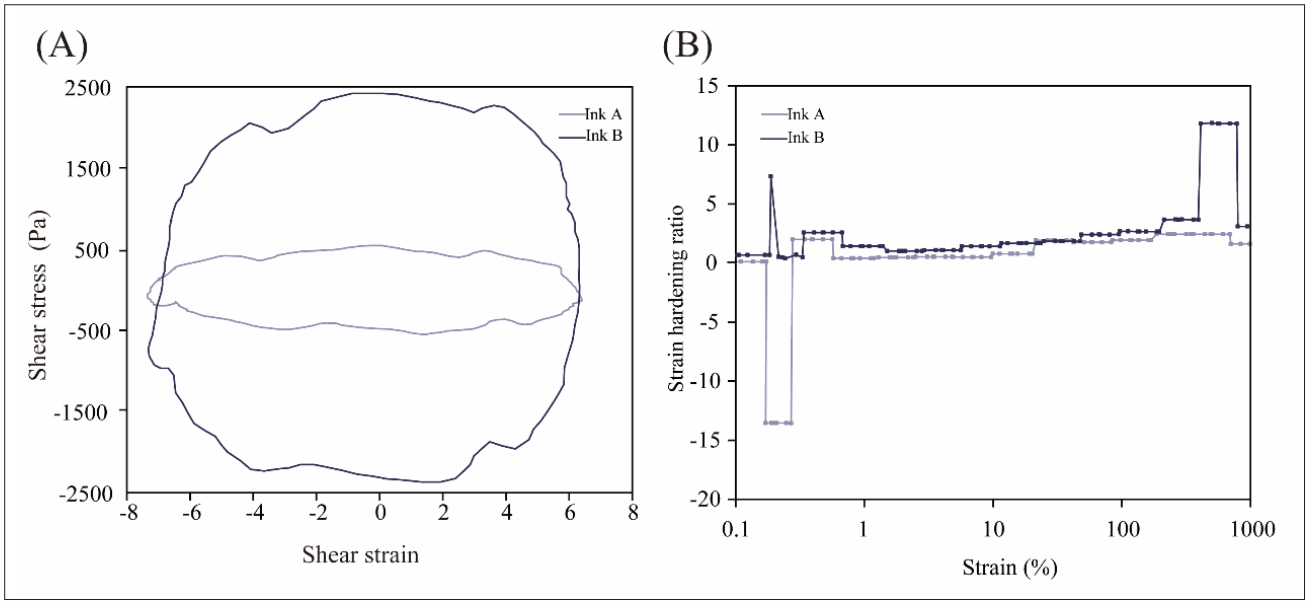

Figure 6. LAOS test results for hydrogel inks. Lissajous curve (A) and strain-hardening curve (B) for ink A (cellulose/collagen I/alginate hydrogel) and B (oxidized cellulose/collagen I/alginate hydrogel). Abbreviation: LAOS: Large amplitude oscillation sweep.

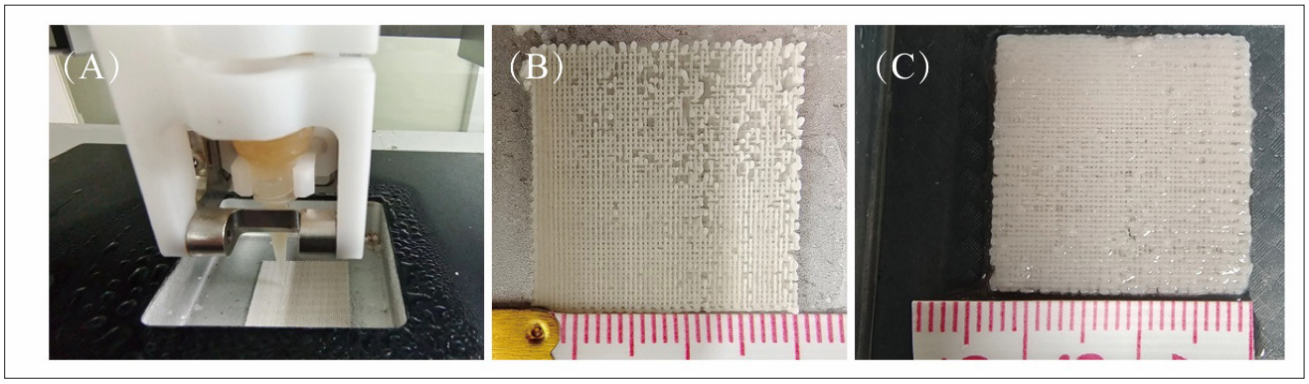

Figure 7. Macroscale images of hydrogel scaffolds. (A) Cryogenic 3D printing setup. (B) 3D-printed scaffold using ink A (cellulose/collagen I/alginate hydrogel). (C) 3D-printed scaffold using ink B (oxidized cellulose/collagen I/alginate hydrogel). The edge length of each scaffold square is 24 mm.

Table 1. Average rod diameter and pore size of scaffold samples before and after swelling

Sample	Before swelling		After swelling	
	Rod diameter (μm)	Pore size (μm)	Rod diameter (μm)	Pore size (μm)
1	158±13	65±13	174±21	140±19
2	173±27	144±42	149±26	192±36
3	184±24	222±16	259±33	350±29
4	237±22	233±17	228±22	324±24

Note: Data are presented as mean ± standard deviations (n = 3).

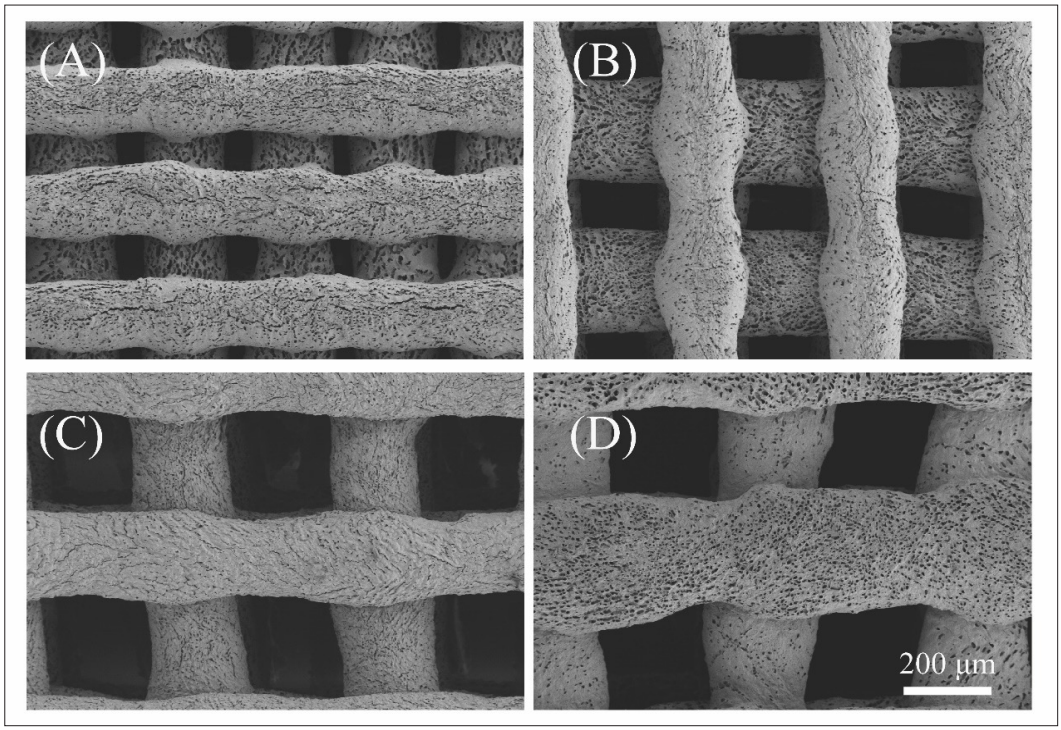

Figure 8. Microscale SEM images of crosslinked scaffolds. (A) Sample 1; (B) Sample 2; (C) Sample 3; (D) Sample 4. The scale bar shown is applicable to all panels. Abbreviation: SEM: Scanning electron microscopy.

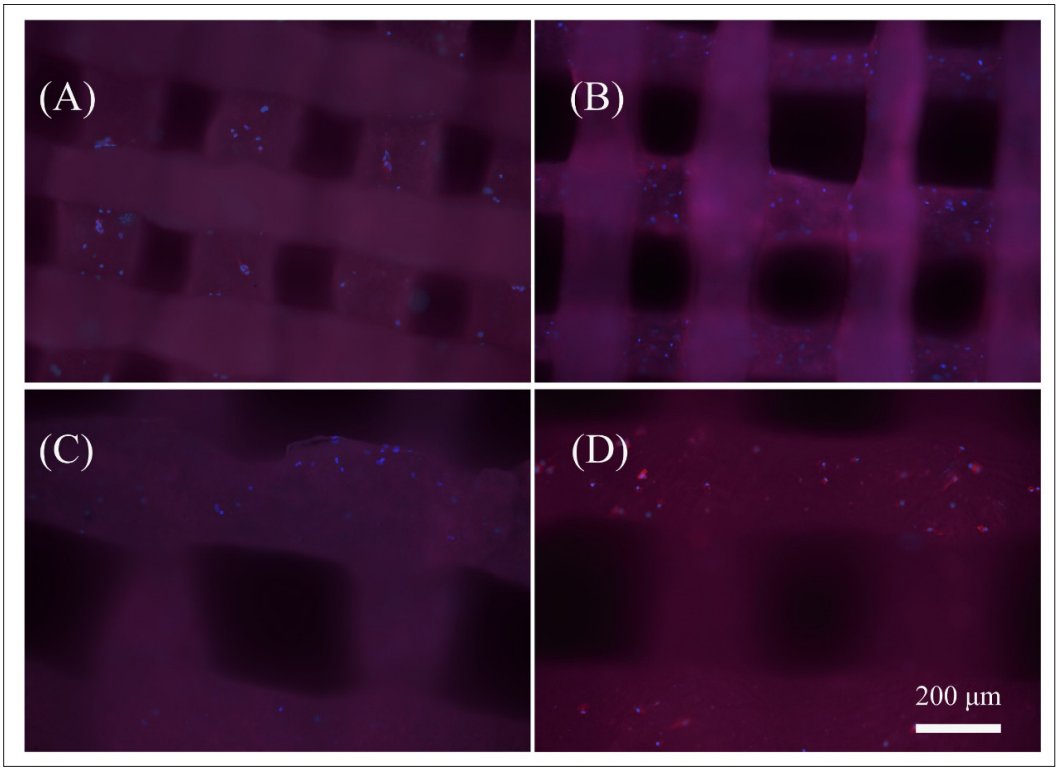

Figure 9. Microscale images of scaffolds seeded with MSCs and stained with DAPI and actin. (A) Sample 1; (B) Sample 2; (C) Sample 3; (D) Sample 4. The scale bar shown is applicable to all panels. Abbreviations: DAPI: 4'6-diamidino-2-phenylindole; MSCs: Mesenchymal stem cells.

and structural integrity of the scaffolds relied primarily on the intrinsic rheological properties of the hydrogel inks, including viscosity, viscoelasticity, and linear rheology. As discussed in **Section 3.2.**, ink B demonstrated enhanced linear rheological characteristics of ink B—presumably due to Schiff-base interaction—which contributed to its superior shape fidelity.

3.4. Mechanical study

Tensile testing was conducted on scaffolds from samples 1–4, and the average elastic moduli were calculated from the linear regions of the stress–strain curves (Figure 11). The moduli were 11.41 ± 0.18 MPa (sample 1), 7.02 ± 1.35 MPa (sample 2), 6.99 ± 0.49 MPa (sample 3), and 4.75 ± 1.84 MPa (sample 4). The highest modulus in sample 1 can be attributed to its smallest rod diameter and pore size, which increased the number of crosslinking junctions and improved resistance to deformation under tensile stress.

3.5. Cell study

On day 5, the OD value of sample 1 was lower than both samples 2 and 3 (Figure 12), which was presumably caused by its lower porosity. According to the western blot (WB) results, the expression of OCN and ALP was the highest in sample 2, indicating the highest level of osteogenic differentiation of MSCs. The NCAD and HIF-1α expressions were also elevated in sample 2, reflecting a higher level of cell condensation and a more hypoxic condition. Lastly, the expression of β-catenin, an osteogenic-related marker, was also most upregulated in sample 2 (Figure 13).

4. Discussion

4.1. Ink rheological properties, printing quality, and post-treatments

Typically, the viscosity and rigidity of hydrogel inks, as measured through steady shear flow and oscillatory rheological tests, are used to evaluate shape fidelity during printing.[24] These are often conducted at a constant strain within the linear elastic region of the ink (0.5–1%).[36] When the hydrogel ink was printed at a relatively low speed, the induced strain remained within this linear range, making such tests appropriate for measuring shape fidelity. However, higher printing resolution often requires significantly higher speed, which can generate large strains—sometimes exceeding 100%.[14] Under such large

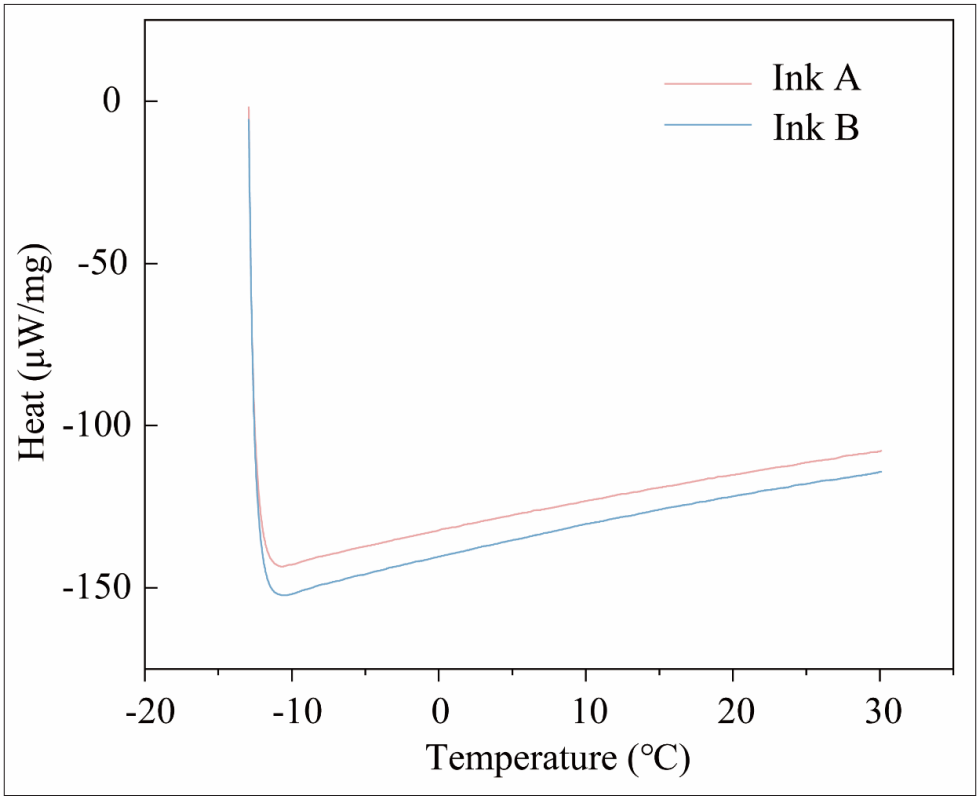

Figure 10. DSC heat flow curve for ink A (cellulose/collagen I/alginate hydrogel) and B (oxidized cellulose/collagen I/alginate hydrogel). Abbreviation: DSC: Differential scanning calorimetry.

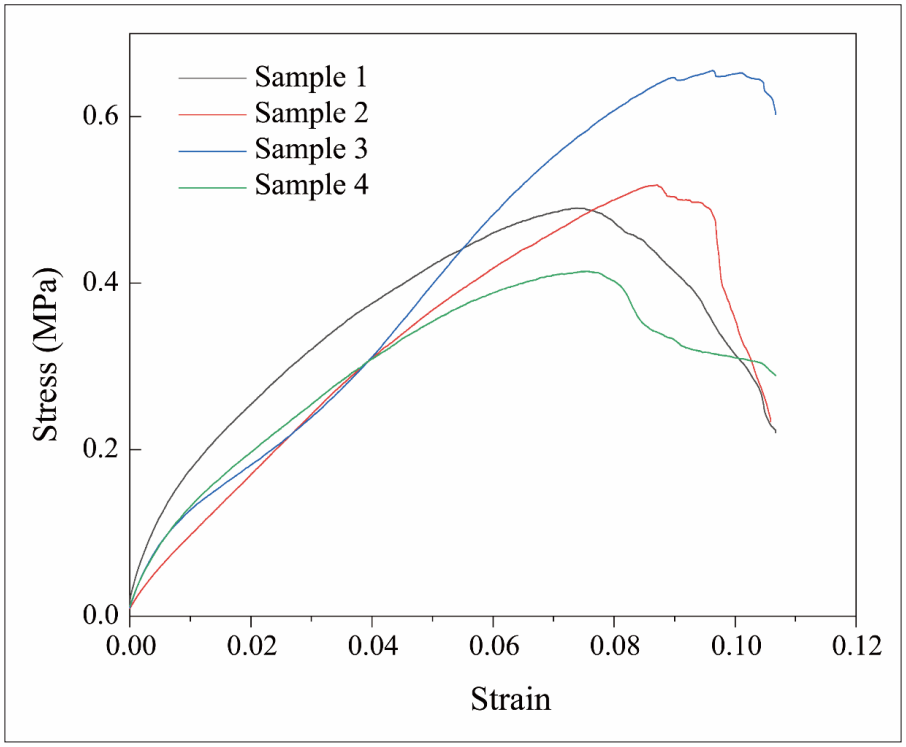

Figure 11. Stress–strain curves of the four scaffold samples

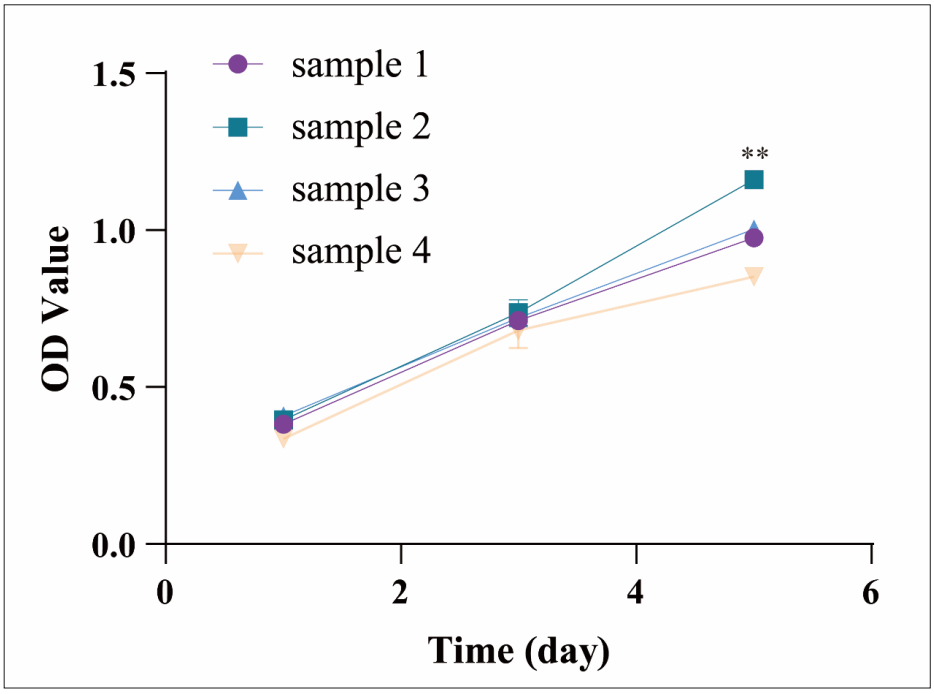

Figure 12. CCK-8 results for the scaffold samples on days 1–5. Data are presented as mean ($n = 3$); ** $p < 0.01$ (compared to control group). Abbreviations: CCK: cell counting kit; DSC: Differential scanning calorimetry.

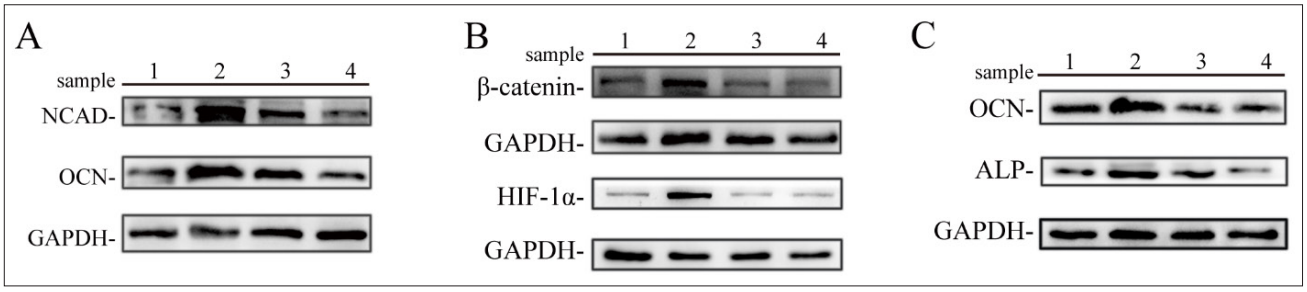

Figure 13. WB images for the four scaffold samples. (A) Expression of NCAD and OCN on day 7. (B) Expression of HIF-1α and β-catenin on day 7. (C) Expression of OCN and ALP on day 21. Abbreviations: ALP, alkaline phosphatase; HIF-1α, hypoxia inducible factor-1α; NCAD, N-cadherin; OCN, osteocalcin; WB, western blot.

strain conditions, LAOS testing provides a more accurate reflection of the ink's rheological behaviors.

Our results showed that although ink A demonstrated higher viscosity and stiffness under low-strain conditions (0.5%), it exhibited weaker linear rheological characteristics across the wider strain range (1–1000%). Linear rheology refers to the regime where stress is directly proportional to strain, resembling the behavior of an ideal Hookean spring.[37] In contrast, inks with strong non-linear behavior resemble viscous fluids and are less able to maintain internal stress under deformation.[38,39] Therefore, inks with stronger linear rheological behavior, such as ink B, are better suited for maintaining structural integrity during high-speed printing. This was further supported by the higher strain-hardening ratio observed in ink B.

The formation of the Schiff-base interaction may disturb the entanglement of collagen I macromolecules and reduce viscosity. Under a larger strain, however, the bonding strength of the Schiff base could be stronger than that of the collagen entanglement. Presumably, due to this reason, ink B with this Schiff-base interaction exhibited a stronger linear rheological characteristic and improved shape fidelity.

In this study, we utilized a moderate cryogenic printing condition at −1, which was unlikely to cause the denaturation of collagen I. According to previous studies, the collagen-to-gelatin transition must involve a heating process,[1,40,41] which was opposite to the temperature condition in cryogenic printing. There are also studies utilizing freeze-drying (at −20°C or lower) to produce collagen-based foam scaffolds, followed by cell and animal studies, indicating that the bioactivity of collagen composition was maintained.[42–45]

For the crosslinking reaction, genipin was used in this study. The reaction involves the bonding of its aldehyde group to the amine group of collagen and gelatin. In other words, the reaction only changes the terminal chemical groups of collagen and gelatin molecules, rather than changing their molecular structure or conformation.[46,47] Therefore, the use of genipin was unlikely to induce denaturation of collagen I. Genipin, a naturally derived crosslinker obtained from the plant *Gardenia jasminoides* Ellis, has been used in traditional Chinese medicine for a long time.[48,49] It has been utilized as a biocompatible and cell-friendly crosslinker to replace synthetic crosslinkers with toxicity, such as formaldehyde and glutaraldehyde.[50] Therefore, it has been used as a routine and standardized crosslinker in drug delivery and post-treatment of biopolymer 3D printing in many studies.[6,51–59] Based on the CCK-8 test results in our study, MSCs proliferated over time, which confirmed that genipin was non-toxic to cells.

4.2. Effects of scaffold structure on cell proliferation

In this study, MSC proliferation was highest in sample 2 from day 1 to day 5. It had a smaller pore size than samples 3 and 4, which likely provided a larger surface area for cell attachment and improved the seeding efficiency and density of MSCs. Though sample 1 had the smallest pore size among all, its pores were even smaller than the rod diameter, rendering a low overall porosity. This limited porosity may have hindered the diffusion of solvents carrying water, nutrition, and metabolic waste, potentially affecting cell proliferation.[60]

In short, our results were inconsistent with some existing studies regarding the effect of pore size on cell proliferation. For example, Sun et al.[61] found that polycaprolactone scaffolds with a medium pore size (350 μm) promoted the proliferation of MSCs more than those with smaller (150 μm) and larger (750 μm) pores. Diao et al.[62] found that tricalcium phosphate scaffolds with a pore size of 300 μm promoted MSC proliferation more than those with 100 and 500 μm-size pores. In contrast, in our study, the pore size at 144 μm exhibited the highest level of cell proliferation. We believe this difference was attributable to the type of scaffold biomaterials. Compared to rigid thermoplastic biopolymers and bioceramics, the

hydrogel scaffolds used in this study were viscoelastic and hydrophilic, and therefore, more favorable for cell adhesion and migration.[63–65] Additionally, the collagen I composition had the surface RGD groups that guided and promoted cell adhesion, and it was also superior in nutrient adsorption during cell culture. Presumably due to these reasons, the use of the collagen I-based hydrogel could "switch" the optimum pore size to a smaller dimension.

In recent years, gelatin has been routinely used as a key component for producing hydrogel scaffolds, as it is a naturally derived protein with a surface RGD group like collagen.[14,26,29,66–70] Though gelatin-based scaffolds have shown significantly improved outcomes in cell adhesion and proliferation compared to metal and thermoplastic biopolymers,[14,71] they remain inferior to scaffolds containing collagen I for bone tissue engineering. Compared to gelatin, collagen I is a native component of bone and has been shown to have a greater osteogenic-promoting effect.[5,72,73] Therefore, we achieved a high printing resolution with a hydrogel ink containing 8% w/v collagen I, which improved the biochemical and structural properties of the scaffolds and could synergistically promote osteogenic differentiation of MSCs. Therefore, our work steps further than recent studies utilizing gelatin-based scaffolds.

4.3. Possible mechanism related to the effect of scaffold structure on osteogenic differentiation

To our best knowledge, studies on the effects of structure on osteogenic differentiation are generally lacking in mesh scaffolds. In the few studies applying scaffolds with relatively big pore sizes (300–700 μm), the level of osteogenic differentiation increased monotonically in smaller pores within this range.[74] However, it is still necessary to produce scaffolds with much higher resolution to further explore their potential to promote osteogenic differentiation and investigate the possible underlying mechanisms.

In this study, the level of osteogenic differentiation was higher in sample 3 than in sample 4, indicating the advantage of using collagen I over gelatin. Among the collagen I-based scaffolds, sample 2 led to the highest level of osteogenic differentiation compared to samples 3 and 4. According to our WB test results, the expression of NCAD was the highest in sample 2, indicating the highest level of cell condensation and cell–cell communication, which could promote osteogenic differentiation, as reported in existing studies.[75–77] Additionally, the expression of NCAD was also the highest in sample 2 and maybe another contributor to promoting osteogenic differentiation.[78] Since MSC proliferation was highest in sample 2, it presumably led to a higher cell density, which promoted cell condensation and the formation of a hypoxic condition. These factors may have contributed to the upregulated expression of NCAD and HIF-1α. In addition, the expression of β-catenin was also highest in sample 2, and the upregulation of this factor has been shown to promote osteogenic differentiation in multiple studies.[79] We believe these findings could deepen our understanding of how scaffold dimensions and structures influence osteogenic differentiation and shed light on the possible mechanisms involved.

4.4. Broader impact of our study in bone tissue engineering

We believe the findings of this study offer several important contributions to the field of bone tissue engineering. First, our results provide insight into resolving the long-standing trade-off between cell proliferation and osteogenic differentiation in scaffold design.[62,68,74,80] Conventionally, smaller pores (100–150 μm) are known to promote osteogenic differentiation, but they often hinder cell proliferation. In bone tissue engineering, both factors are important: while higher proliferation increases the total production of ECM components, differentiation determines the proportion of bone-specific ECM components.[81,82] More importantly, our results indicated that higher cell proliferation may actually promote osteogenic differentiation by upregulating the expression of NCAD and HIF-1α. This highlights the importance of addressing both proliferation and differentiation in tandem rather than in isolation. In this study, such a trade-off was successfully solved in sample 2, which exhibited the highest levels of both proliferation and osteogenic differentiation, indicating that an optimal pore size can support both processes simultaneously.

Second, our work addresses a key challenge in scaffold development: the difficulty of optimizing both the compositional and structural properties for bone regeneration. Although collagen I is widely regarded as one of the most favorable biomaterials for bone tissue engineering,[83] previous studies have either failed to fabricate high-resolution collagen I-based mesh scaffolds or have achieved high-resolution scaffolds using alternative materials such as bioplastics, metals, or ceramics.[6,84,85] In our study, we addressed the printability limitations of collagen I-based hydrogels by introducing a Schiff-base interaction, which enhanced ink rheology and enabled the successful printing of high-resolution scaffolds. This allowed us to simultaneously optimize both composition and structure, enhancing the scaffold's performance in supporting bone regeneration.

Lastly, much of the recent progress in bone tissue engineering has focused on biochemical enhancements, such as incorporating novel growth factors to stimulate osteogenesis.[86–89] In contrast, studies focusing on structural

optimization have been relatively limited, presumably due to material processing constraints and insufficient scaffold resolution to promote osteogenic differentiation.[14] While growth factors can be effective, their use often introduces added cost, complexity in formulation and release control, and potential safety concerns, all of which pose challenges for clinical translation.[90] Our results demonstrate that by achieving a high printing resolution with a collagen I-based scaffold, it is possible to promote both cell proliferation and osteogenic differentiation without relying on external biochemical agents. This presents a more straightforward and potentially more clinically translatable approach. We believe this study will inspire further exploration into the role of scaffold's structural characteristics in promoting bone tissue regeneration.

5. Conclusion

In this study, we successfully addressed the limited printability of collagen I-based hydrogels by incorporating a Shiff-base interaction, enabling the fabrication of high-resolution scaffolds with rod diameters and pore sizes below 200 μm. This improved printing resolution was primarily attributed to an enhanced linear rheological characteristic of the hydrogel ink, rather than an increase in viscosity. We also identified an optimal combination of pore size and rod diameter that simultaneously promoted MSC proliferation and osteogenic differentiation. Mechanistic insights revealed that these effects were associated with the upregulation of NCAD, HIF-1α, and β-catenin expression. To conclude, we successfully designed and fabricated scaffolds with both optimized compositional and structural characteristics to support the proliferation and osteogenic differentiation of MSCs. We believe this study broadens our understanding of scaffold design and optimization, offering valuable insights for future applications in bone tissue engineering.

Acknowledgments

The authors would like to thank the Center for Scientific Research of Anhui Medical University for their valuable assistance in the experiments.

Funding

This work was supported by the National Natural Science Foundation of China (82272551), Hefei Comprehensive National Science Center Institute of Health and Medicine (JKS2023001), and the University Natural Science Research Project of Anhui Province (2022AH051152).

Conflict of interest

The authors declare no competing interests.

Author contributions

Conceptualization: Hanxiao Huang
Funding acquisition: Cailiang Shen
Investigation: Kaixuan Li, Hanxiao Huang, Peng Ge
Methodology: Kaixuan Li, Hanxiao Huang
Formal analysis: Kaixuan Li
Writing–original draft: Kaixuan Li, Hanxiao Huang
Writing–review & editing: Kaixuan Li, Cailiang Shen

Ethics approval and consent to participate

All animal work involved in this study was approved by Experimental Animal Ethics Committee of Anhui Medical University (Approval no.: LLSC20250455).

Consent for publication

Not applicable.

Availability of data

Data is available from the corresponding author upon reasonable request.

References

1. Dille MJ, Haug IJ, Draget KI. Chapter 34—gelatin and collagen. In: Phillips GO, Williams PA, eds. *Handbook of Hydrocolloids*. 3rd ed. Duxford, United Kingdom: Woodhead Publishing; 2021:1073-1097.

2. Marques CF, Diogo GS, Pina S, Oliveira JM, Silva TH, Reis RL. Collagen-based bioinks for hard tissue engineering applications: a comprehensive review. *J Mater Sci Mater Med*. 2019;30(3):32
doi: 10.1007/s10856-019-6234-x.

3. Hersel U, Dahmen C, Kessler H. RGD modified polymers: biomaterials for stimulated cell adhesion and beyond. *Biomaterials*. 2003;24(24):4385-4415.
doi: 10.1016/S0142-9612(03)00343-0

4. Ruoslahti E, Pierschbacher MD. New perspectives in cell adhesion: RGD and integrins. *Science*. 1987;238(4826):491-497
doi: 10.1126/science.2821619.

5. Kim NR, Lee DH, Chung P-H, Yang H-C. Distinct differentiation properties of human dental pulp cells on collagen, gelatin, and chitosan scaffolds. *Oral Surg Oral Med Oral Pathol Oral Radiol Endod*. 2009;108(5):e94-e100.
doi: 10.1016/j.tripleo.2009.07.031.

6. Suo H, Zhang J, Xu M, Wang L. Low-temperature 3D printing of collagen and chitosan composite for tissue engineering. *Mater Sci Eng C*. 2021;123(12): 111963.

doi: 10.1016/j.msec.2021.111963.

7. Bacakova L, Novotna K, Hadraba D, Musilkova J, Slepicka P, Beran M. Influence of biomimetically mineralized collagen scaffolds on bone cell proliferation and immune activation. *Polymers*. 2022;14(3):602. doi: 10.3390/polym14030602

8. Dewey MJ, Johnson EM, Slater ST, Milner DJ, Wheeler MB, Harley BA, Mineralized collagen scaffolds fabricated with amniotic membrane matrix increase osteogenesis under inflammatory conditions. *Regen Biomater*. 2020;7(3):247-258. doi: 10.1093/rb/rbaa005

9. Eviana Putri NR, Wang X, Chen Y, Li X, Kawazoe N, Chen G. Preparation of PLGA-collagen hybrid scaffolds with controlled pore structures for cartilage tissue engineering. *Prog Nat Sci Mater Int*. 2020;30(5):642-650. doi: 10.1016/j.pnsc.2020.07.003.

10. Gómez-Guillén MC, Giménez B, López-Caballero ME, Montero MP. Functional and bioactive properties of collagen and gelatin from alternative sources: a review. *Food Hydrocoll*. 2011;25(8):1813-1827. doi: 10.1016/j.foodhyd.2011.02.007.

11. Gurumurthy B, Janorkar AV. Improvements in mechanical properties of collagen-based scaffolds for tissue engineering. *Curr Opin Biomed Eng*. 2021;17:100253. doi: 10.1016/j.cobme.2020.100253.

12. Kokol V, Pottathara YB, Mihelčič M, Perše LS. Rheological properties of gelatine hydrogels affected by flow- and horizontally-induced cooling rates during 3D cryo-printing. *Colloids Surf A Physicochem Eng Asp*. 2021;616(3):126356. doi: 10.1016/j.colsurfa.2021.126356.

13. Gautieri A, Vesentini S, Redaelli A, Buehler MJ. Viscoelastic properties of model segments of collagen molecules. *Matrix Biol*. 2012;31(2):141-149. doi: 10.1016/j.matbio.2011.11.005.

14. Huang H, Li K, Hou J, Shen C. A study of the temperature-dependent stress yielding behavior of a gelatin-based hydrogel ink and its effects on the enhancement of the 3D printing resolution. *Polym Test*. 2024;137(3):108501. doi: 10.1016/j.polymertesting.2024.108501.

15. Sobral JM, Caridade SG, Sousa RA, Mano JF, Reis RL. Three-dimensional plotted scaffolds with controlled pore size gradients: effect of scaffold geometry on mechanical performance and cell seeding efficiency. *Acta Biomater*. 2011;7(3):1009-1018. doi: 10.1016/j.actbio.2010.11.003.

16. Harley BAC, Kim HD, Zaman MH, Yannas IV, Lauffenburger DA, Gibson LJ. Microarchitecture of three-dimensional scaffolds influences cell migration behavior via junction interactions. *Biophys J*. 2008;95(8):4013-4024. doi: 10.1529/biophysj.107.122598.

17. Lee H, Yang GH, Kim M, Lee J, Huh J, Kim G. Fabrication of micro/nanoporous collagen/dECM/silk-fibroin biocomposite scaffolds using a low temperature 3D printing process for bone tissue regeneration. *Mater Sci Eng C*. 2018;84:140-147. doi: 10.1016/j.msec.2017.11.013

18. Yang L, Jin S, Shi L, et al. Cryogenically 3D printed biomimetic scaffolds containing decellularized small intestinal submucosa and Sr2+/Fe3+ co-substituted hydroxyapatite for bone tissue engineering. *Chem Eng J*. 2022;431(4):133459. doi: 10.1016/j.cej.2021.133459

19. Jiang S, Yu Z, Zhang L, et al. Effects of different aperture-sized type I collagen/silk fibroin scaffolds on the proliferation and differentiation of human dental pulp cells. *Regen Biomater*. 2021;8(4):rbab028. doi: 10.1093/rb/rbab028.

20. Kim G, Ahn S, Yoon H, Kim Y, Chun W. A cryogenic direct-plotting system for fabrication of 3D collagen scaffolds for tissue engineering. *J Mater Chem*. 2009;19(46):8817-8823. doi: 10.1039/B914187A.

21. Dutta SD, Hexiu J, Patel DK, Ganguly K, Lim KT. 3D-printed bioactive and biodegradable hydrogel scaffolds of alginate/gelatin/cellulose nanocrystals for tissue engineering. *Int J Biol Macromol*. 2021;167:644-658. doi: 10.1016/j.ijbiomac.2020.12.011.

22. Liu D, Dong X, Han B, Huang H, Qi M. Cellulose nanocrystal/collagen hydrogels reinforced by anisotropic structure: shear viscoelasticity and related strengthening mechanism. *Comp Commun*. 2020;21:100374. doi: 10.1016/j.coco.2020.100374.

23. Zhang W, Shi K, Yang J, et al. 3D printing of recombinant collagen/chitosan methacrylate/nanoclay hydrogels loaded with Kartogenin nanoparticles for cartilage regeneration. *Regen Biomater*. 2024;11:rbae097. doi: 10.1093/rb/rbae097.

24. Townsend JM, Beck EC, Gehrke SH, Berkland CJ, Detamore MS. Flow behavior prior to crosslinking: the need for precursor rheology for placement of hydrogels in medical applications and for 3D bioprinting. *Prog Polym Sci*. 2019;91(43):126-140. doi: 10.1016/j.progpolymsci.2019.01.003.

25. Huang H, Dean D. 3-D printed porous cellulose acetate tissue scaffolds for additive manufacturing. *Addit Manuf*. 2020;31:100927. doi: 10.1016/j.addma.2019.100927

26. Wang Y, Yang S, Cai H, et al. A dual-crosslinking electroactive hydrogel based on gelatin methacrylate and dibenzaldehyde-terminated telechelic polyethylene glycol for 3D bio-printing. *Sci Rep*. 2024;14(1):4118. doi: 10.1038/s41598-024-54853-9.

27. Heid S, Becker K, Byun J, et al. Bioprinting with bioactive alginate dialdehyde-gelatin (ADA-GEL) composite bioinks: time-dependent in-situ crosslinking via addition of calcium-

silicate particles tunes in vitro stability of 3D bioprinted constructs. *Bioprinting*. 2022;26:e00200. doi: 10.1016/j.bprint.2022.e00200.

28. Jiang Y, Zhou J, Yang Z, et al. Dialdehyde cellulose nanocrystal/gelatin hydrogel optimized for 3D printing applications. *J Mater Sci*. 2018;53(16):11883-11900. doi: 10.1007/s10853-018-2407-0.
29. Aghajanzadeh MS, Imani R, Nazarpak MH. In situ forming aldehyde-modified xanthan/gelatin hydrogel for tissue engineering applications: synthesis, characterization, and optimization. *J Mater Sci*. 2023;58(35):14187-14206. doi: 10.1007/s10853-023-08878-6.
30. Cheng Q-P, Hsu S-h. A self-healing hydrogel and injectable cryogel of gelatin methacryloyl-polyurethane double network for 3D printing. *Acta Biomater*. 2023; 164(3):124-138. doi: 10.1016/j.actbio.2023.04.023.
31. Tohamy H-AS, Taha G, Sultan M. Dialdehyde cellulose/ gelatin hydrogel as a packaging material for manganese oxides adsorbents for wastewater remediation: characterization and performance evaluation. *Int J Biol. Macromol*. 2023;248:125931. doi: 10.1016/j.ijbiomac.2023.125931.
32. Lu Y, Zhao M, Peng Y, et al. A physicochemical double-cross-linked gelatin hydrogel with enhanced antibacterial and anti-inflammatory capabilities for improving wound healing. *J Nanobiotechnol*. 2022;20(1):426. doi: 10.1186/s12951-022-01634-z.
33. Kim MH, Lee YW, Jung W-K, Oh J, Nam SY. Enhanced rheological behaviors of alginate hydrogels with carrageenan for extrusion-based bioprinting. *J Mech Behav Biomed Mater*. 2019;98:187-194. doi: 10.1016/j.jmbbm.2019.06.014.
34. Basu P, Saha N, Saha P. Swelling and rheological study of calcium phosphate filled bacterial cellulose-based hydrogel scaffold. *J Appl Polym Sci*. 2020;137(14):48522. doi: 10.1002/app.48522
35. Li Q, Xu S, Feng Q, et al. 3D printed silk-gelatin hydrogel scaffold with different porous structure and cell seeding strategy for cartilage regeneration. *Bioact Mater*. 2021;6(10):3396-3410. doi: 10.1016/j.bioactmat.2021.03.013.
36. Huang H, Ayariga J, Ning H, Nyairo E, Dean D. Freeze-printing of pectin/alginate scaffolds with high resolution, overhang structures and interconnected porous network. *Addit Manuf*. 2021;4:102120. doi: 10.1016/j.addma.2021.102120.
37. Townsend AK, Wilson HJ. Small- and large-amplitude oscillatory rheometry with bead–spring dumbbells in Stokesian dynamics to mimic viscoelasticity. *J Non-Newton Fluid Mech*. 2018;261(1):136-152. doi: 10.1016/j.jnnfm.2018.08.010.
38. Hyun K, Wilhelm M, Klein CO, et al. A review of nonlinear oscillatory shear tests: analysis and application of large amplitude oscillatory shear (LAOS). *Prog Polym Sci*. 2011;36(12):1697-1753. doi: 10.1016/j.progpolymsci.2011.02.002.
39. Wang Y, Selomulya C. Food rheology applications of large amplitude oscillation shear (LAOS). *Trends Food Sci Technol*. 2022;127(4):221-244. doi: 10.1016/j.tifs.2022.05.018.
40. Liu D, Nikoo M, Boran G, Zhou P, Regenstein JM. Collagen and gelatin. *Annu Rev Food Sci Technol*. 2015;6:527-557. doi: 10.1146/annurev-food-031414-111800.
41. Komsa-Penkova R, Koynova R, Kostov G, Tenchov B. Discrete reduction of type I collagen thermal stability upon oxidation. *Biophys Chem*. 2000;83(3):185-195. doi: 10.1016/S0301-4622(99)00135-0.
42. Offeddu GS, Ashworth JC, Cameron RE, Oyen ML. Structural determinants of hydration, mechanics and fluid flow in freeze-dried collagen scaffolds. *Acta Biomater*. 2016;41:193-203. doi: 10.1016/j.actbio.2016.05.024.
43. Varley MC, Neelakantan S, Clyne TW, Dean J, Brooks RA, Markaki AE. Cell structure, stiffness and permeability of freeze-dried collagen scaffolds in dry and hydrated states. *Acta Biomater*. 2016;33:166-175. doi: 10.1016/j.actbio.2016.01.041.
44. O'Brien FJ, Harley BA, Yannas IV, Gibson L. Influence of freezing rate on pore structure in freeze-dried collagen-GAG scaffolds. *Biomaterials*. 2004;25(6):1077-1086. doi: 10.1016/S0142-9612(03)00630-6.
45. Sionkowska A, Kozłowska J. Properties and modification of porous 3-D collagen/hydroxyapatite composites. *Int J Biol Macromol*. 2013;52(1):250-259. doi: 10.1016/j.ijbiomac.2012.10.002.
46. Solorio L, Zwolinski C, Lund AW, Farrell MJ, Stegemann JP. Gelatin microspheres crosslinked with genipin for local delivery of growth factors. *J Tissue Eng Regen Med*. 2010;4(7):514-523. doi: 10.1002/term.267.
47. Nickerson MT, Patel J, Heyd DV, Rousseau D, Paulson AT. Kinetic and mechanistic considerations in the gelation of genipin-crosslinked gelatin. *Int J Biol Macromol*. 2006;39(4):298-302. doi: 10.1016/j.ijbiomac.2006.04.010.
48. Manickam B, Nair R, Elumalai M. 'Genipin' – the natural water soluble cross-linking agent and its importance in the modified drug delivery systems: an overview. *Curr Drug Deliv*. 2014;11(1):139. doi: 10.2174/15672018113106660059.
49. Adamiak K, Sionkowska A. Current methods of collagen cross-linking: review. *Int J Biol Macromol*. 2020;161(8):550-560.

doi: 10.1016/j.ijbiomac.2020.06.075.

50. Gao L, Gan H, Meng Z, et al. Effects of genipin cross-linking of chitosan hydrogels on cellular adhesion and viability. *Colloids Surf B Biointerfaces*. 2014;117:398–405. doi: 10.1016/j.colsurfb.2014.03.002.

51. Oustadi F, Imani R, Haghbin Nazarpak M, Sharifi AM. Genipin-crosslinked gelatin hydrogel incorporated with PLLA-nanocylinders as a bone scaffold: synthesis, characterization, and mechanical properties evaluation. *Polym Adv Technol*. 2020;31(8):1783-1792. doi: 10.1002/pat.4905.

52. Zafeiris K, Brasinika D, Karatza A, et al. Additive manufacturing of hydroxyapatite–chitosan–genipin composite scaffolds for bone tissue engineering applications. *Mater Sci Eng C*. 2021;119:111639. doi: 10.1016/j.msec.2020.111639.

53. Kim YB, Lee H, Kim GH. Strategy to achieve highly porous/biocompatible macroscale cell blocks, using a collagen/genipin-bioink and an optimal 3D printing process. *ACS Appl Mater Interfaces*. 2016;8(47):32230-32240. doi: 10.1021/acsami.6b11669.

54. Hafezi F, Scoutaris N, Douroumis D, Boateng J. 3D printed chitosan dressing crosslinked with genipin for potential healing of chronic wounds. *Int J Pharm*. 2019;560:406-415. doi: 10.1016/j.ijpharm.2019.02.020.

55. Yu Y, Xu S, Li S, Pan H. Genipin-cross-linked hydrogels based on biomaterials for drug delivery: a review. *Biomater Sci*. 2021;9(5):1583-1597. doi: 10.1039/D0BM01403F.

56. Shao Y, Gan N, Gao B, He B. Sustainable 3D-printed β-galactosidase immobilization coupled with continuous-flow reactor for efficient lactose-free milk production. *Chem Eng J*. 2024;481:148557. doi: 10.1016/j.cej.2024.148557.

57. Liu F, Li W, Liu H, et al. Preparation of 3D printed chitosan/polyvinyl alcohol double network hydrogel scaffolds. *Macromol Biosci*. 2021;21(4):2000398. doi: 10.1002/mabi.202000398.

58. Erben A, Hörning M, Hartmann B, et al. Precision 3D-printed cell scaffolds mimicking native tissue composition and mechanics. *Adv Healthc Mater*. 2020;9(24):2000918. doi: 10.1002/adhm.202000918.

59. Saito-Diaz K, Dietrich P, Saini T, et al. Genipin rescues developmental and degenerative defects in familial dysautonomia models and accelerates axon regeneration. *Sci Transl Med*. 2024;16(774):eadq2418. doi: 10.1126/scitranslmed.adq2418.

60. Luo C, Wang C, Wu X, et al. Influence of porous tantalum scaffold pore size on osteogenesis and osteointegration: a comprehensive study based on 3D-printing technology. *Mater Sci Eng C*. 2021;129(5):112382. doi: 10.1016/j.msec.2021.112382.

61. Sun Y, Wu Q, Zhang Y, Dai K, Wei Y. 3D-bioprinted gradient-structured scaffold generates anisotropic cartilage with vascularization by pore-size-dependent activation of HIF1α/FAK signaling axis. *Nanomed Nanotechnol Biol Med*. 2021;37(5):102426. doi: 10.1016/j.nano.2021.102426.

62. Diao J, OuYang J, Deng T, et al. 3D-plotted beta-tricalcium phosphate scaffolds with smaller pore sizes improve in vivo bone regeneration and biomechanical properties in a critical-sized calvarial defect rat model. *Adv Healthc Mater*. 2018;7(17):1800441. doi: 10.1002/adhm.201800441.

63. Bauer A, Gu L, Kwee B, et al. Hydrogel substrate stress-relaxation regulates the spreading and proliferation of mouse myoblasts. *Acta Biomater*. 2017;62(7):82-90. doi: 10.1016/j.actbio.2017.08.041.

64. Ma Y, Han T, Yang Q, et al. Viscoelastic cell microenvironment: hydrogel-based strategy for recapitulating dynamic ECM mechanics. *Adv Funct Mater*. 2021;31(24):2100848. doi: 10.1002/adfm.202100848.

65. Chaudhuri O, Cooper-White J, Janmey PA, Mooney DJ, Shenoy VB, Effects of extracellular matrix viscoelasticity on cellular behaviour. *Nature*. 2020;584(7822):535-546. doi: 10.1038/s41586-020-2612-2.

66. Serag E, Eltawila AM, Salem EM, El-Maghraby A, Abd El-Aziz AM. Development of an innovative cylindrical carbon nanofiber/gelatin-polycaprolactone hydrogel scaffold for enhanced bone regeneration. *Int J Biol Macromol*. 2025;306(8):141250. doi: 10.1016/j.ijbiomac.2025.141250.

67. Kalogeropoulou M, Díaz-Payno PJ, Mirzaali MJ, van Osch GJVM, Fratila-Apachitei LE, Zadpoor AA. 4D printed shape-shifting biomaterials for tissue engineering and regenerative medicine applications. *Biofabrication*. 2024;16(2):022002. doi: 10.1088/1758-5090/ad1e6f.

68. Kim H, Yang GH, Choi C, Cho Y, Kim G. Gelatin/PVA scaffolds fabricated using a 3D-printing process employed with a low-temperature plate for hard tissue regeneration: fabrication and characterizations. *Int J Biol Macromol*. 2018;120:119-127. doi: 10.1016/j.ijbiomac.2018.07.159.

69. Wu S-C, Chang W-H, Dong G-C, Chen K-Y, Chen Y-S, Yao C-H. Cell adhesion and proliferation enhancement by gelatin nanofiber scaffolds. *J Bioact Compat Polym*. 2011;26(6):565-577. doi: 10.1177/0883911511423563.

70. Wang J, Dongyang Z, Guangchao W, et al. Enhanced bone regeneration with bioprinted GelMA/Bentonite scaffolds inspired by bone matrix. *Virtual Phys Prototyp*. 2024;19(1):e2345765.

doi: 10.1080/17452759.2024.2345765.

71. Salehi Abar E, Vandghanooni S, Torab A, Jaymand M, Eskandani M. A comprehensive review on nanocomposite biomaterials based on gelatin for bone tissue engineering. *Int J Biol Macromol.* 2024;254(1):127556. doi: 10.1016/j.ijbiomac.2023.127556.

72. Xu L, Anderson AL, Lu Q, Wang J. Role of fibrillar structure of collagenous carrier in bone sialoprotein-mediated matrix mineralization and osteoblast differentiation. *Biomaterials*. 2007;28(4):750-761. doi: 10.1016/j.biomaterials.2006.09.022.

73. Shi H, Li Y, Xu K, Yin J. Advantages of photo-curable collagen-based cell-laden bioinks compared to methacrylated gelatin (GelMA) in digital light processing (DLP) and extrusion bioprinting. *Mater Today Bio*. 2023;23(5):100799. doi: 10.1016/j.mtbio.2023.100799.

74. Di Luca A, Ostrowska B, Lorenzo-Moldero I, et al. Gradients in pore size enhance the osteogenic differentiation of human mesenchymal stromal cells in three-dimensional scaffolds. *Sci Rep*. 2016;6(1):22898. doi: 10.1038/srep22898.

75. Xu L, Meng F, Ni M, Lee Y, Li G. N-cadherin regulates osteogenesis and migration of bone marrow-derived mesenchymal stem cells. Mol Biol Rep. 2013;40(3):2533-2539. doi: 10.1007/s11033-012-2334-0.

76. Zhu M, Lin S, Sun Y, Feng Q, Li G, Bian L. Hydrogels functionalized with N-cadherin mimetic peptide enhance osteogenesis of hMSCs by emulating the osteogenic niche. *Biomaterials*. 2016;77:44-52. doi: 10.1016/j.biomaterials.2015.10.072.

77. Guntur AR, Rosen CJ, Naski MC. N-cadherin adherens junctions mediate osteogenesis through PI3K signaling. *Bone*. 2012;50(1):54-62. doi: 10.1016/j.bone.2011.09.036.

78. Burzi IS, Parchi PD, Barachini S, et al. Hypoxia promotes the stemness of mesangiogenic progenitor cells and prevents osteogenic but not angiogenic differentiation. *Stem Cell Rev Rep*. 2024;20(7):1830-1842. doi: 10.1007/s12015-024-10749-9.

79. Hu L, Chen W, Qian A, Li Y-P. Wnt/β-catenin signaling components and mechanisms in bone formation, homeostasis, and disease. *Bone Res.* 2024;12(1):39. doi: 10.1038/s41413-024-00342-8.

80. Swanson WB, Omi M, Zhang Z, et al. Macropore design of tissue engineering scaffolds regulates mesenchymal stem cell differentiation fate. *Biomaterials*. 2021;272(1):120769. doi: 10.1016/j.biomaterials.2021.120769.

81. Koons GL, Diba M, Mikos AG. Materials design for bone-tissue engineering. *Nat Rev Mater*. 2020;5(8):584-603. doi: 10.1038/s41578-020-0204-2

82. James AW. Review of signaling pathways governing MSC osteogenic and adipogenic differentiation. *Scientifica* 2013;2013(1):684736. doi: 10.1155/2013/684736.

83. Vijayalekha A, Anandasadagopan SK, Pandurangan AK. An overview of collagen-based composite scaffold for bone tissue engineering. *Appl Biochem Biotechnol.* 2023;195(7):4617-4636. doi: 10.1007/s12010-023-04318-y.

84. Li Y, Liu Y, Li R, et al. Collagen-based biomaterials for bone tissue engineering. *Mater Des.* 2021;210(7):110049. doi: 10.1016/j.matdes.2021.110049.

85. Mu X, Agostinacchio F, Xiang N, et al. Recent advances in 3D printing with protein-based inks. *Prog Polym Sci*. 2021;115:101375. doi: 10.1016/j.progpolymsci.2021.101375.

86. Ho-Shui-Ling A, Bolander J, Rustom LE, Johnson AW, Luyten FP, Picart C. Bone regeneration strategies: engineered scaffolds, bioactive molecules and stem cells current stage and future perspectives. *Biomaterials*. 2018;180:143-162. doi: 10.1016/j.biomaterials.2018.07.017.

87. Zhao H-y, Wu J, Zhu J-j, et al. Research advances in tissue engineering materials for sustained release of growth factors. *BioMed Res Int.* 2015;2015(6):808202. doi: 10.1155/2015/808202

88. De Witte T-M, Fratila-Apachitei LE, Zadpoor AA, Peppas NA. Bone tissue engineering via growth factor delivery: from scaffolds to complex matrices. *Regen Biomater*. 2018;5(4):197-211. doi: 10.1093/rb/rby013

89. Shrivats AR, McDermott MC, Hollinger JO. Bone tissue engineering: state of the union. *Drug Discov Today*, 2014;19(6):781-786. doi: 10.1016/j.drudis.2014.04.010.

90. Oryan A, Alidadi S, Moshiri A, Bigham-Sadegh A. Bone morphogenetic proteins: a powerful osteoinductive compound with non-negligible side effects and limitations. *BioFactors*. 2014;40(5):459-481. doi: 10.1002/biof.1177.